THE JOURNAL OF PHYSICAL CHEMISTRY B

ARTICLE

pubs.acs.org/JPCB

Liquid Methanol Confined within Functionalized Silica Nanopores. 2. Solvation Dynamics of Coumarin 153

M. Dolores Elola,*[,†] Javier Rodriguez,[†,‡] and Daniel Laria[†,§]

[†]Departamento de Física, Comisión Nacional de Energía Atómica, Avenida Libertador 8250, 1429 Buenos Aires, Argentina.

[‡]ECyT, UNSAM, Martín de Irigoyen 3100, 1650 San Martín, Provincia de Buenos Aires, Argentina

[§]Departamento de Qumica Inorgánica Analítica y Química-Física e INQUIMAE, Facultad de Ciencias Exactas y Naturales, Universidad de Buenos Aires, Ciudad Universitaria, Pabellón II. 1428 Buenos Aires, Argentina

ABSTRACT: Equilibrium and dynamical characteristics pertaining to the solvation of the fluorescent probe coumarin 153 in liquid methanol confined within cylindrical silica pores are investigated using molecular dynamics techniques. Three kinds of pores are examined: (i) Soft hydrophobic cavities, in which wall−solvent interactions were exclusively of the Lennard-Jones type; (ii) Hydrophilic cavities, in which unsaturated oxygen sites at the wall were transformed into hydroxyl groups; (iii) Rugged pores, in which 60% of the polar groups were transformed into bulkier and mobile trimethylsilyl moieties. Equilibrium solvation structures in the three pores differ considerably: In hydrophobic environments, the solute remains adsorbed to the pore wall, with its molecular plane mostly parallel to the interface. Upon hydroxylation, the solid interface becomes preferentially coated by methanol, leading to a bistable solvation state of the probe, with alternation of "wall-like" and "bulk-like" events. An increment in the interface roughness promotes a solvation structure characterized by the embedding of the probe within a wall domain surrounded by trimethylsilyl groups. In hydrophobic environments, the relevant dynamical modes of the probe can be cast in terms of in-the-wall rotations, whereas in hydrophilic pores, out-of-the-wall evolutions are also present. The embedding of the probe at wall domains in more rugged pores, leads to restrained angular motions, with maximum amplitudes of the order of 20°. Results of early stages of the solvation response of the environment following a vertical excitation of the probe are also presented. During the initial 30 ps, we found no evidence of modifications in the spatial localizations of the probe. The overall responses are found to be between 2 and 4.5 times slower than the one observed in the bulk, being the fastest relaxation the one associated to rugged pores whereas the slowest one corresponds to hydrophilic cavities. These features are rationalized in terms of the composition of the first solvation shells and the local dynamical inhomogeneities prevailing within the different regions of the pores.

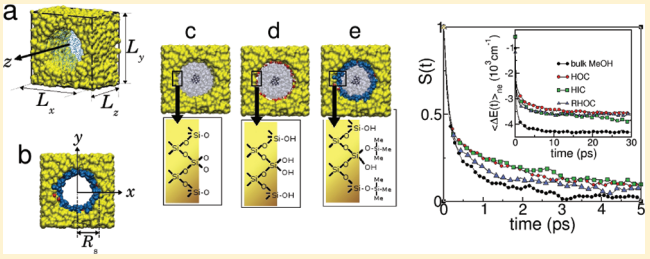

I. INTRODUCTION

The behavior of liquids under geometrical confinement remains a very active research area in nanoscience. The interest in these phases has been spurred by the dramatic modifications that take place in the structural and dynamical features of these systems, when the length scales that characterize the overall confinement become comparable to typical molecular sizes. These modifications are manifested in a wide variety of equilibrium and dynamical properties. From a microscopic perspective, the former involve modifications in the intra- and intermolecular spatial correlations between the different species comprising the confined liquid. In some cases, these modifications can even give rise to more global responses, such as the appearance of new phases, which are absent in more conventional, condensed phases.[1,2] On the dynamical side, the overall effects are normally perceived by the important stretchings exhibited by practically all the characteristic time scales describing thermal fluctuations within restrained environments.[3]

The present paper examines equilibrium and dynamical characteristics of the solvation of the fluorescent probe coumarin 153 (C153) in liquid methanol (MeOH), confined within three different kinds of cylindrical silica pores with diameters ∼3 nm. Our analysis relied on the implementation of molecular dynamics (MD) simulations. C153 (see Figure 1) represents a versatile dye molecule that has been used in many previous studies to unveil microscopic details of a variety of liquid environments, such as polar and nonpolar phases,[4−6] reverse micelles,[7] supercritical states,[8] ionic liquids,[9,10] protein−surfactant complexes,[11] and confined polar liquids,[12,13] to provide a few relevant examples.

Our motivation to perform the present simulation experiments was 2-fold: on the one hand, the recent publication of a new series of results of steady-state and time-resolved fluorescence spectra of the C153 dissolved in different aliphatic alcohols in silica pores by Kamijo et al.;[13] previously, dynamical information about the solvation of the probe in liquid ethanol confined within sol−gel glasses had also been reported by Baumann

Received: June 21, 2011
Revised: August 26, 2011
Published: September 20, 2011

ACS Publications © 2011 American Chemical Society

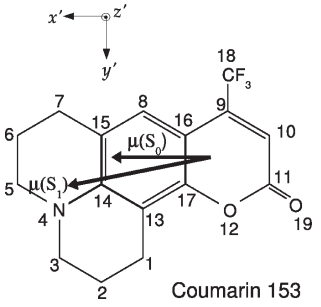

Figure 1. Atom numbering used for C153. The dipole moment vectors corresponding to the ground (S_0) and excited (S_1) states are also displayed on top of the molecule.

et al.[12] On the other hand, the present paper represents a complement to a previous molecular dynamics study, in which we analyzed equilibrium and dynamical aspects of pure MeOH trapped within cylindrical pores.[14] It is well-known that simulation techniques represent an optimal tool to gain physical insight about the mechanisms that control the solvent responses that follow the modifications operated in the electronic distribution of a tagged solute.[5,15−19] In particular, this information is crucial for the adequate interpretation of the early stages of such relaxations which, due to inherent restrictions in the time resolution of the experimental techniques, may remain partially elusive. The list of previous simulation studies dealing with the analysis of the solvation dynamics in confined systems includes environments such as pores,[20−24] reverse micelles[25] and cyclodextrin cavities[26] as well.

In the present case, we have incorporated a high degree of atomistic detail in our model Hamiltonian. In doing so, we try to capture some key ingredients that, we believe, are fundamental to reach an adequate interpretation of a complex phenomenon whose dynamics is controlled not only by the dynamical modes of the solvent, i.e., the usual bulk-like scenario but also by those describing fluctuations in the spatial location and orientational state of the probe within the pore. As we will see, the latter effects, in turn, are indirectly connected to the prevailing interactions between the pore wall, the probe and the solvent molecules.

The organization of the paper is as follows: In section II we summarize the details of the model and the technical aspects of the simulation procedure. Section III contains the main results of our study in which we examine equilibrium and dynamical features of the probe. The concluding remarks are left for section IV.

II. MODELS AND COMPUTATIONAL DETAILS

The systems under investigation were composed of a single C153 probe localized within cylindrical silica nanopores filled with liquid methanol (MeOH). The silica pores were generated following a procedure described in full detail in previous papers.[14,23,27,28] Briefly, we started by considering a sample of fused SiO_2, with density 2.2 g cm^{-3}, contained within a fully periodic, rectangular simulation box of linear dimensions $L_x = L_y = 51$ Å and $L_z = 33$ Å, equilibrated at a temperature close to $T \approx 8000$ K. After immobilizing a central cylindrical section of radius $R_s = 16.5$ Å along the z axis, the surrounding portion was allowed to cool down to ambient conditions, by multiple rescaling of the atomic velocities. The central portion of the sample was then removed, leaving a cylindrical pore of radius R_s, across the silica

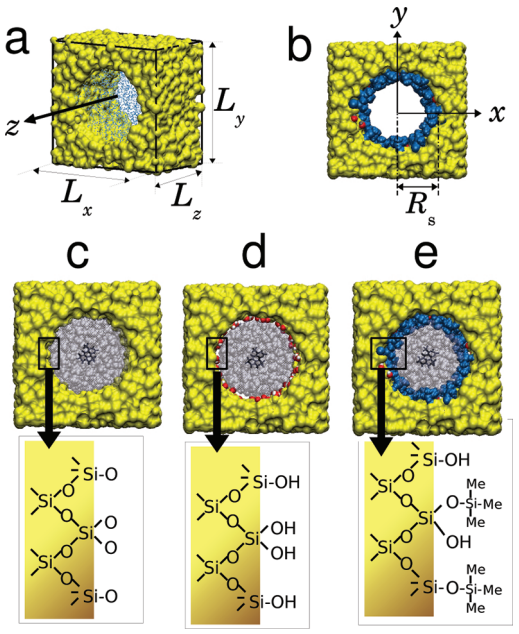

Figure 2. Top panels (a) and (b) show the orientation of the simulation box relative to the laboratory axes; R_s is the radius of the silica pore. On bottom panels, snapshots of "bulk solvation states" configurations for (c) HOC, (d) HIC, and (e) RHOC simulated silica nanopores are shown, along with the schematic illustration of the pore wall functionalization.

block. At ambient conditions, these samples exhibited structural and dynamical characteristics similar to those of amorphous solids (see parts a and b of Figure 2). The next stage of the preparation involved bringing the silica pore, with the C153 fixed at its center, adjacent to a previously equilibrated reservoir containing ∼1800 MeOH molecules. In doing so, the length of the simulation box along the z axis was initially enlarged up to ∼80 Å. As the solvent was allowed to permeate through the pore, L_z was finally adjusted so as to bring the MeOH density away from the pore in agreement with the bulk value at ambient conditions. From then on, the adjacent reservoir was removed and all constraints acting on the probe were released.[14]

Three kinds of pores, differing in the effective solid−liquid and solid−C153 interactions were examined:[14,28] (i) A hydrophobic cavity (HOC), in which dispersive, i.e., Lennard-Jones, forces prevail. (ii) A hydrophilic cavity (HIC), in which a sizable number of unsaturated O groups at the pore surface was transformed into polar −OH groups. In order to reproduce data obtained from experimental absorption experiments,[13] the surface density of silanol groups was set to ∼3 nm^{-2}. (iii) Finally, we also examined MeOH confinement within a much more rugged—and intermediate, in terms of of its hydrophobic characteristics—cavity (RHOC), in which 60% of the surface −OH groups were replaced by bulkier and mobile O−Si−$(CH_3)_3$ trimethylsilyl (TMS) groups. We remark that, in all cases, after the annealing procedure, all atoms in the solid block remained immobile, with the exception of the hydrogen sites in the silanol groups and those comprising the TMS moieties. Typical snapshots of the three simulated silica cavities are shown in parts c−e of Figure 2.

Inter- and intramolecular parameters for interactions involving MeOH molecules were taken from the fully flexible, CHARMM27 force field.[29] The total intermolecular interaction

Table 1. Number of Selected Species Comprising the Simulated Systems

			cavity type		
	species	bulk	HOC	HIC	RHOC
N_{C153}	coumarin 153	1	1	1	1
N_{MeOH}	CH_3OH	530	368	385	256
N_{SiOH}	SiOH			86	32
N_{TMS}	$SiOSi(CH_3)_3$				55

consisted of a sum of Lennard-Jones plus Coulombic site−site contributions. The fluorescent probe was also modeled as a fully flexible, 10 Å × 6 Å planar structure, comprising 36 interaction sites (see Figure 1). Intermolecular parameters were taken from the force field used in a previous work,[26] whereas partial charges for the ground and excited states were taken from ab initio calculations performed by Martins and Skaf (see Table 1 of ref 30). This parametrization yields dipolar moments for C153 in bulk methanol μ_{S_0} = 7.3 D and μ_{S_1} = 15.2 D for the ground and excited states, respectively. Reported values from dielectric measurements yield a value of 6.55 D for the ground-state dipole moment,[31] while electro-optic studies reveal that the excited-state dipole moment is intermediate between 14 and 16 D, depending on the particular solvent considered.[32] Lennard-Jones length and energy parameters for the C153 were taken from ref 17. Finally, inter- and intramolecular potential parameters involving Si, O, silanol, and TMS groups in the solid substrate can be found in ref 28.

Two kinds of simulation experiments were performed: (i) equilibrium averages of relevant observables related to the solvation of C153 in the ground state were collected along a 20 ns, microcanonical, trajectory; (ii) nonequilibrium runs, in which the original charge distribution of the coumarin was switched, at t = 0, to that corresponding to the excited state. Initial conditions for these runs were taken from statistically independent configurations of the ground state trajectory, separated by 25 ps intervals. From these nonequilibrium initial configurations, the relaxations of the system were followed for about 30 ps.

All molecular dynamics trajectories were generated using the NAMD package.[33] Periodic boundary conditions were applied along the three Cartesian coordinates. Short-ranged intermolecular forces were cut off at 15 Å, while the particle mesh Ewald (PME) method was implemented to handle long-range Coulomb forces. The equations of motions were integrated using a multiple time step integration scheme, with a time step of 1 fs for intramolecular modes, 2 fs for nonbonded short-ranged forces, and 4 fs for the rest of the Coulomb forces. After filling the different silica cavities with the MeOH solution, preliminary equilibration trajectories at $T \approx 298$ K, lasting typically ~500 ps, were discarded. From then on, configurations were saved every 0.5 ps along 20 ns trajectories for data analysis. Table 1 displays the numbers of molecules employed in each system.

III. RESULTS

A. Dynamics in the Nanosecond Time Domain. To gain a preliminary insight on the characteristics of the solvation of the probe within the pore, we will start by examining the time evolution of a few relevant parameters along a 20 ns, equilibrium trajectory, with the probe in the S_0 state. Since the pore represents an inhomogeneous environment for the solvation, perhaps the first and simplest question to be answered concerns the overall location of the probe. In the top panels of Figures 3, 4, and 5, we have displayed the time evolution of the distance

$$R_{cm}(t) = \sqrt{X_{cm}^2(t) + Y_{cm}^2(t)} \quad (1)$$

where $X_{cm}(t)$ and $Y_{cm}(t)$ represent Cartesian coordinates of the C153 center of mass at time t, measured from the position of the axis of the pore. As a general trend, it is clear that, in the three systems, the probe lies mostly in the outer, i.e., $R_{cm} \gtrsim 10$ Å, liquid layer. Clearly, the former "wall-solvation-states" (WSS) are entropically benefited with respect to "bulk-solvation-states" (BSS), localized at more central regions of the pore.

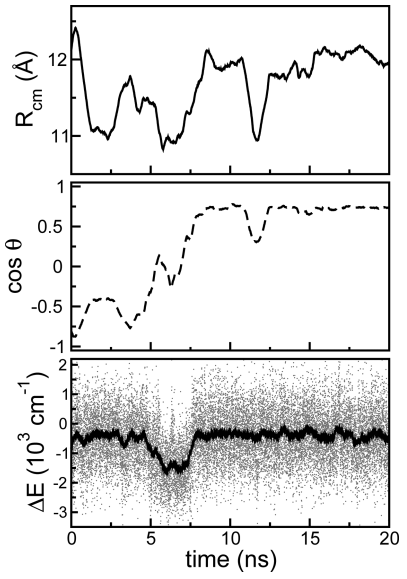

Figure 3. Time evolution of different observables from equilibrium MD simulations with the coumarin in the ground state, for the HOC system. Top panel: distance between the coumarin center-of-mass and the axial axis of the cylindrical cavity. Middle panel: cosine of the tilt angle θ. Bottom panel: total energy gap $\Delta E(t)$ (gray dots) and $\overline{\Delta E}(t)$ (solid line); the latter corresponds to the gap averaged out over 500 points (i.e., 0.5 ns).

Still, some differences can be established between these external solvation states: when compared to those prevailing in HOC and RHOC scenarios, wall−C153 interactions in HICs appear somewhat weaker. Note that in the hydrophilic pore, the probe detaches from the solid−liquid interface at $t \approx 11$ ns and remains localized at the center of pore ($R_{cm} \approx 5$ Å) during the subsequent 5 ns, before performing a 2 ns excursion back to more external environments. Finally, a closer inspection of the time behavior of $R_{cm}(t)$ in RHOC suggests a stronger stabilization near the wall, as its relevant fluctuations hardly exceeds 0.25 Å.

The previous observations can be complemented with the analysis of the rotational dynamics of the probe. To that end, we monitored the behavior of

$$\cos\theta = \frac{\mathbf{R}_{cm}}{|\mathbf{R}_{cm}|} \cdot \hat{\mathbf{z}}' \quad (2)$$

where $\hat{\mathbf{z}}'$ is a unit vector normal to the C153 molecular plane (see Figure 1). The plot in the middle panel of Figure 3 shows that, in HOCs, that plane remains mostly in contact with the pore wall.

dx.doi.org/10.1021/jp205832y |J. Phys. Chem. B 2011, 115, 12859–12867

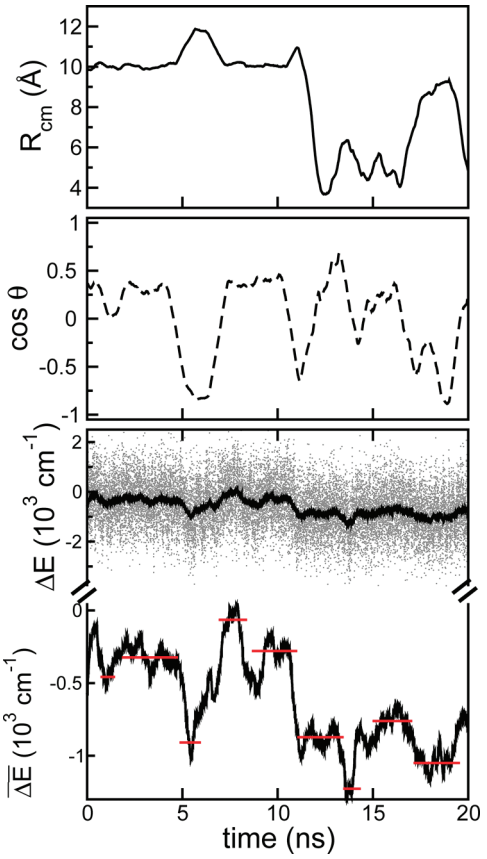

Figure 4. Same as Figure 3 for the HIC system. The bottom panel includes zoomed results for $\overline{\Delta E(t)}$, for better clarity. The horizontal segments indicate averages of $\overline{\Delta E(t)}$ taken along short temporal intervals of the order of the nanosecond (see text).

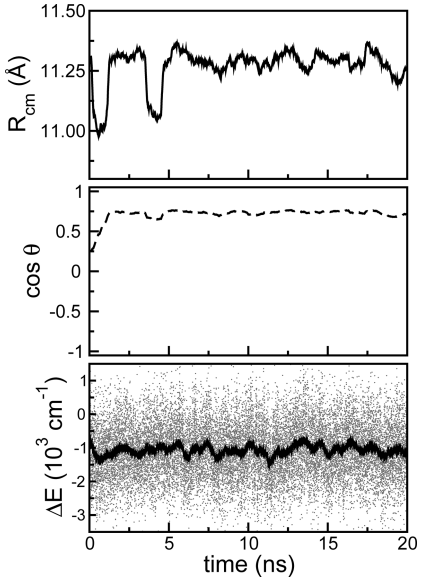

Figure 5. Same as Figure 3 for the RHOC system.

At $t \approx 3$ ns, a flip of the contact plane takes place, which requires 4−5 ns to be fully achieved. On the other hand, in HICs, WSS and BSS are both characterized by a permanent loss of parallelism (middle panel of Figure 4). Finally, in RHOCs, the overall orientational fluctuations drop dramatically, as the probe gets "anchored" within a wall domain, surrounded by TMS groups which, in turn, severely hamper the out-of-the-wall rotational dynamics of the probe.

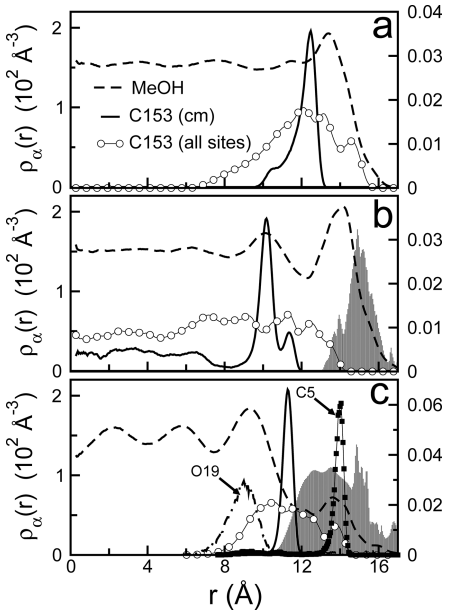

Figure 6. Local density profiles along the radial direction, for methanol (dashed line, left *y*-axis), coumarin center-of-mass (solid line, right *y*-axis) and all coumarin sites (line with circles, right *y*-axis). The profiles were obtained from an equilibrium trajectory with the coumarin in the ground-state. Panels a, b, and c correspond to the HOC, HIC, and RHOC systems. The coumarin profiles with circles have been multiplied by a factor of 2 for better visualization. The shaded curves on panels b and c correspond to the hydrogen sites of SiOH groups and CH_3 sites of TMS groups.

B. Equilibrium Solvation Structures. Spatial and time correlations provide a more quantitative description of the gross features described in previous paragraphs. Figure 6 includes results for local density fields of the type

$$\rho_\alpha(r) = \frac{1}{2\pi r L_z} \sum_i \langle \delta(r - R_i^\alpha) \rangle \qquad (3)$$

where R_i^α denotes the distance of the center of mass of the *i*th molecule of species α to the pore axis. The density profiles of methanol species look similar to those already discussed in previous work,[14] in which pure methanol was investigated confined within similar silica cavities. For the sake of completeness, we summarize the main features of these plots: in HOCs and in HICs, one observes central regions of radii $r \lesssim 11$ Å and $r \lesssim 8$ Å, respectively, where the local density profiles remain practically structureless, at a value $\rho_{MeOH}(r) \approx \rho_{bulk}$. Near the silica wall, fluctuations are also clearly perceived and characterized by local maxima at $r = 13$ Å and $r \approx 14$ Å. In addition, hydroxylation promotes a larger extent of liquid structure toward the interior of the pore (note a second peak at $r \approx 10$ Å). Fluctuations are even more marked in RHOCs, where the corresponding profile of $\rho_{MeOH}(r)$ exhibits an outer solvent shell, represented by a much smaller surface peak at $r \approx 13.5$ Å

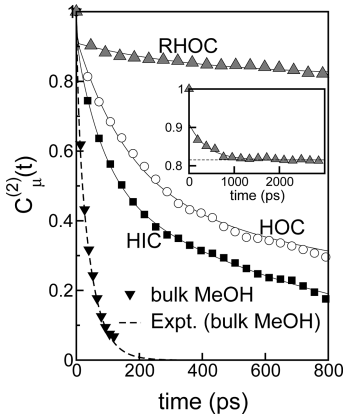

Figure 7. Second-rank single-dipole time correlation function of ground-state C153 in bulk and confined MeOH (with symbols). Solid lines represent the fitting functions. Experimental data were taken from ref 6, measured in the excited state from fluorescence depolarization techniques. The inset shows the RHOC curve on a larger time scale, along with the asymptotic plateau value in dashed lines.

and an interface-induced spatial ordering which extends much deeper into the liquid phase.

Concerning the position of the C153, the profiles corresponding to the center of mass and to averages taken over the whole set of atomic positions, present the following features: (i) WSS in HOCs and RHOCs are characterized by single peaks of $\rho_{C153}(r)$ located at $r \approx 11-12$ Å, being the width for the latter case much narrower than the one for the HOC case. (ii) The analysis of the distribution for the complete set of interaction sites of C153 in RHOCs reveals that the probe remains adsorbed with the C5 flank embedded within domains surrounded by TMS moieties and exposing the C11−O19 carbonyl group to the solvent (C153 site labeling appears in Figure 1). (iii) In HICs, the main peak of the center of mass distribution moves to an inner solvent shell, centered at $r \approx 10$ Å. (iv) Moreover, the distribution for the complete set of C153 sites also remains shifted to lower values of r, indicating that the pore wall is coated exclusively by MeOH which, in turn, is stabilized by wall−solvent hydrogen bonding. (v) Finally, the latter distribution also includes a left-hand-side branch that stretches down to the center of the pore, which corresponds to BSS.

C. Rotational Dynamics of Confined C153. Our analysis of the orientational degrees of freedom of the probe will be focused on their dynamical characteristics. Time resolved fluorescent anisotropy measurements normally provide information about the depolarization dynamics, which can be cast in terms of single-dipole time correlation functions of the type

$$C_\mu^{(2)}(t) = \langle P_2[\cos\theta_\mu(t)]\rangle \tag{4}$$

with

$$\cos\theta_\mu(t) = \frac{\boldsymbol{\mu}(0)\cdot\boldsymbol{\mu}(t)}{|\boldsymbol{\mu}^2|} \tag{5}$$

In eq 4, $P_2(x) = (3x^2 - 1)/2$ is the second-rank Legendre polynomial and $\mu(t)$ in eq 5 represents the instantaneous transition dipole moment of the C153.[34] Figure 7 shows the rotational TCFs obtained for the C153 in the S_0 state, in the different silica nanopores. As a reference, the figure also includes simulation results for C153 in bulk methanol, which

Table 2. Fit Parameters for the Second-Rank Rotational Correlation Functions $C_\mu^{(2)}(t)$ and for the Solvation Functions $S(t)$, for C153 in Bulk and Confined Methanol[a]

	rotational dynamics						solvation dynamics[c]			
	a_1	τ_1	a_2	τ_2	τ_{rot}	$\tau_{rot}/\tau_{rot}^{bulk}$	a_1	τ_1	τ_{slv}	$\tau_{slv}/\tau_{slv}^{bulk}$
HOC	0.45	2097	0.55	152	1027	28	0.22	5.69	1.47	2.8
HIC	0.50	825	0.50	71.2	448	12	0.18	13.0	2.37	4.5
RHOC					389[b]	11	0.20	4.64	1.03	1.9

[a] Rotational and solvation times, τ_{rot} and τ_{slv}, were obtained from time integration of $C_\mu^{(2)}(t)$ and $S(t)$, respectively. Times are given in picoseconds. [b] This time corresponds to the fit parameter τ_w of eq 7. [c] Single-exponential fits of $S(t)$ were adjusted for $t \gtrsim 2$ ps.

are in excellent agreement with experimental data obtained by Horng et al.[5]

Rotational characteristics times, τ_{rot}, for C153 localized in the hydrophobic and hydrophilic pores are listed in column 6 of Table 2. The estimates were obtained from time integrals of biexponential fits of the type

$$C_\mu^{(2)}(t) = a_1 \exp(-t/\tau_1) + a_2 \exp(-t/\tau_2) \tag{6}$$

Direct comparison of pore and bulk results shows a significant stretching of the characteristic time scales; τ_{rot} in HICs is 1 order of magnitude larger, while, in hydrophobic cavities, the differences are even more marked, involving a factor of ∼30. Note that this trend could have been somehow anticipated from the simple consideration of the localization of the probe within the pores. In fact, our results suggest that the prevalence of WSSs gets translated into a drastic slowdown of the orientational motions of the probe, whereas the more central localization of the C153 in hydrophilic pores would mitigate confinement effects, bringing the overall characteristics of the rotational motions of the probe somewhat closer to, albeit still slower than, those found in the bulk. Moreover, the prevalence of WSS in HOCs, characterized by the persistence of contact between the plane of the C153 and the pore wall, would indicate that the orientational decorrelation depicted in the $C_\mu^{(2)}(t)$ corresponds to in-the-wall-motions, i.e., rotations around the local z' axis, perpendicular to the molecular plane of the probe (see Figure 1).

The characteristics of $C_\mu^{(2)}(t)$ for RHOCs differentiate from those found for the other two cavities. The inset of Figure 7 indicates that, after a time interval of ∼1 ns, the correlation function levels off at a plateau value close to ∼0.8. We recall that, at the crudest level of representation, the prevailing solvation scenario in these cavities can be portrayed in terms of a pivoting probe, "anchored" at the fixed C5 site.

Given these characteristics, the plateau value of $C_\mu^{(2)}(t)$ can be physically rationalized on more quantitative grounds by resorting to the classical "wobbling-in-a-cone" (WIC) rotational diffusion model, which assumes a free rotational motion of the probe within a constrained conical domain, defined by an azimuthal angle θ_0. Within this context, after a short transient, the expression of $C_\mu^{(2)}(t)$, can be written as

$$C_\mu^{(2)}(t) \approx A_\infty + (1 - A_\infty)\exp(-t/\tau_w) \tag{7}$$

where τ_w defines a wobbling diffusional time scale proportional to the inverse of the rotational diffusion constant. As such, assuming a random distribution of orientations within the cone,

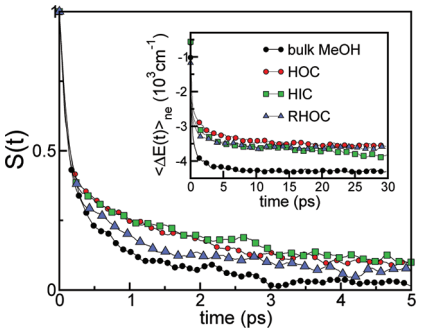

Figure 8. Normalized solvation response function for coumarin 153 confined within silica nanopores, obtained from averages of 400 nonequilibrium independent trajectories. The inset shows the corresponding unnormalized energy gaps, $\langle \Delta E(t) \rangle_{ne}$, along the whole time interval 0−30 ps.

the model predicts

$$\lim_{t \to \infty} C_{\mu}^{(2)}(t) \approx \left[\frac{1}{2} \cos \theta_0 (1 + \cos \theta_0) \right]^2 \tag{8}$$

and an expression for the equilibrium fluctuations of the form

$$\Delta \cos \theta = \left[\frac{\cos^2 \theta_0}{12} - \frac{\cos \theta_0}{6} + \frac{1}{12} \right]^{1/2} \tag{9}$$

A least-squares fit of the simulated $C_{\mu}^{(2)}(t)$ yields $A_{\infty} = 0.82$ and $\tau_w = 0.39$ ns, while eqs 8 and 9 predict $\theta_0 \approx 20°$ and via a direct change of variables $\Delta\theta \approx 11°$. We remark that a direct analysis of the time evolution of the orientations of μ along an equilibrium trajectory (not shown) reveals that the magnitude of the angular fluctuations is $\Delta\theta \approx 8°$, in close agreement with the prediction obtained from the WIC model. This observation brings support to a simplified description, based on restrained diffusional orientational motions, with maximum amplitudes of the order of 20°.

D. Solvation Dynamics. Solvation dynamics in polar media can be investigated by time-resolved Stokes shift experiments.[15,35,36] The solvation response is usually reported in terms of the time evolution of $\nu(t)$, the frequency of the maximum of the fluorescence signal, via a normalized response function of the type

$$S(t) = \frac{\nu(t) - \nu(\infty)}{\nu(0) - \nu(\infty)} \tag{10}$$

where $\nu(\infty)$ corresponds to the maximum of the steady-state emission spectrum. Within the context of computer simulation studies, the solvation response can be analyzed by the time-dependent relaxations of the solute−environment electrostatic energy gap[17,37,38]

$$S(t) = \frac{\langle \Delta E(t) - \Delta E(\infty) \rangle_{ne}}{\langle \Delta E(0) - \Delta E(\infty) \rangle_{ne}} \tag{11}$$

where $\Delta E(t)$ represents the environment contribution, i.e., MeOH and pore walls, to the energy gap between the S_1 and S_0 Born−Oppenheimer potential energy surfaces of the probe at time t[17,38]

$$\Delta E(t) = \sum_{\alpha \in C153} \Delta q_{\alpha} V_{\alpha}(t) \tag{12}$$

In the previous equation, Δq_{α} and $V_{\alpha}(t)$ represent the charge jump and the electrostatic potential at the solute site α, respectively

$$V_{\alpha} = \sum_{j \notin C153} \frac{q_j}{r_{\alpha j}} \tag{13}$$

In eq 13, the label j refers to all charged sites in the system, other than those of the probe. Angular brackets of the type $\langle \cdots \rangle_{ne}$ in eq 11 denote an average obtained from a set of nonequilibrium trajectories.

In Figure 8 we present plots for $S(t)$; also included are results for the solvation response in the bulk. We remark that the value of $\Delta E(\infty)$ in the denominator of eq 11 was estimated from an average of $\Delta E(t)$ taken from the $25 \le t \le 30$ ps time interval (the curves in the inset of Figure 8 confirm that the first stages of the relaxation seem to be fully completed beyond, say, 20 ps). At a first glance, the bulk curve clearly detaches from the rest of the much slower pore results which, in turn, exhibit similar relaxation characteristic times. Quantitative estimates of these time scales can be obtained from time integrals of $S(t)$, namely

$$\tau_{slv} = \int_0^{\infty} S(t)\, dt \tag{14}$$

Results for τ_{slv} are listed in column 10 of Table 2. The observed trend reveals that the fastest solvation relaxation corresponds to RHOCs, while the slowest one is found in hydrophilic cavities. Still, and contrasting with the differences observed in the characteristic rotational times, the three values of τ_{slv} in the pores are similar to that of the bulk case (see entries in columns 7 and 11 of Table 2). As such, one can anticipate that the rationalization of these subtle modifications will not be straightforward since the relaxation process incorporates, in a nontrivial fashion, contributions from dynamical modes of the solvent, the probe, and in some cases, a few mobile wall-sites as well. Focusing on the role of the solvent, in a recent publication, we have reported differences of several orders of magnitude between rotational and diffusive characteristics of MeOH molecules localized in the center and in contact with pore wall.[14] Consequently, we cannot discard that the overall MeOH relaxation will integrate contributions from solvent molecules localized in different dynamical domains.

The first important observation that we would like to bring into consideration is that, during the first 20−30 ps following the $S_0 \rightarrow S_1$ transition, we were unable to detect meaningful modifications in the spatial and orientational characteristics of the original probe solvation. The persistence of the original solvation structure has also been reported in a recent analysis of the solvation of C153 within β-cyclodextrins[26] and contrasts with the changes in the spatial localization of excited diatomic molecules confined within spherical cavities reported by Thompson.[21] The absence of modifications in the probe localization would confirm the intricacies controlling the initial and final states of the relaxations, which are the result of a delicate interplay between the characteristics of the local probe−solvent couplings modulated with the prevailing wall-solvent effective interactions.

To provide a plausible interpretation of the results, it will be instructive to pause for a moment to examine the characteristics of $\Delta E(t)$, along the equilibrium trajectories which are shown in the bottom panels of Figures 3, 4, and 5. In the three cases, the temporal scales describing gap fluctuations are in the picosecond

time regime, whereas their magnitudes are close to $\delta(\Delta E) \approx 900\ \mathrm{cm}^{-1}$. Note that the latter values also provide reasonable linear-response estimates[39] for the nonequilibrium energy gap, i.e., $\langle \Delta E(0) - \Delta E(\infty)\rangle_{ne} \approx (k_B T)^{-1}\langle(\delta\Delta E)^2\rangle \approx 4000\ \mathrm{cm}^{-1}$, a value which is close to the one we obtained from nonequilibrium relaxations (see Figure 8). Still, further investigations need to be performed before taking linear response predictions for granted since it has been shown by Ladanyi and Fonseca[40] that the solvation dynamics in bulk methanol exhibits departures from the linear behavior. Anyhow, the presence of such rapid fluctuations precludes a clear identification of additional time scales describing the temporal behavior of the gaps. As a simple way to integrate out these fast modes and shed light into the characteristics of eventual slower ones, we found it convenient to examine averages of the type

$$\overline{\Delta E}(t) = \frac{1}{\Delta}\int_{t-\Delta/2}^{t+\Delta/2} \Delta E(t')\, dt' \qquad (15)$$

where we arbitrarily set Δ to 0.5 ns. In this way, the join inspection of the three panels of Figure 3 makes now the physical interpretation of the behavior of $\overline{\Delta E}(t)$ (also shown in the bottom panel) in HOCs quite direct. At $t \approx 4$ ns, $\overline{\Delta E}$ presents a sharp drop from $\sim -500\ \mathrm{cm}^{-1}$ down to $\sim -1500\ \mathrm{cm}^{-1}$, as the probe makes a full out-of-the-wall-rotation. This increment comes as a consequence of practically doubling the number of solvent molecules lying in the closest solvation shell of the coumarin, as its molecular plane detaches from the pore wall. It is well established that, in the bulk, the main contribution to the solvent gap comes from this closest shell.[37,41]

The temporal evolution of $\overline{\Delta E}(t)$ in the case of hydrophilic pores (bottom panel of Figure 4) looks somewhat different and can be portrayed in terms of a sequence of temporal segments, lasting typically 1−2 ns, interrupted by transitions. As such, there would appear to be a separation of time scales between the ones governing the fast dynamics of ΔE in the course of these segments—most likely reflecting solvent dynamical modes—and those controlling the more sporadic transitions between the segments in $\overline{\Delta E}(t)$. To bring this point more clear, in Figure 4 we have added horizontal bars which indicate averages of $\overline{\Delta E}(t)$ taken along these segments. Note that, in many cases, transitions between the different segments go hand in hand with modifications in the spatial and angular coordinates of the probe (the drop episodes at $t \approx 5$ ns and at $t \approx 11$ ns are self-evident), indicating that they might be controlled mostly by dynamical modes of the probe. Finally in RHOC, the overall profile of $\overline{\Delta E}(t)$ looks featureless and practically uncorrelated from fluctuations in the spatial localization and the orientational state of the probe, revealing that they might not be sufficiently large to modify the temporal behavior $\overline{\Delta E}(t)$ at a qualitative level, in a sensible fashion

Given this scenario, four important conclusions are worth commenting: (i) In pore environments, our simulation results show that the solvation response in the picosecond time domain is clearly slower than the one observed in the bulk. Moreover, functionalization effects may stretch these differences up to approximately 5 times. These modifications in the time scales are comparable to those reported in time dependent Stokes shift experiments of C153 dissolved in confined ethanol,[42] although the trend—in terms of pore-wall functionalization—is different from the one predicted by our simulations. (ii) We were unable to detect modifications in the spatial and orientation characteristics of the original solvation state due to the vertical $S_0 \rightarrow S_1$ transition. (iii) Yet, translational and rotational modes of the probe do affect the dynamics of $\overline{\Delta E}(t)$ along an equilibrium trajectory, introducing fluctuations that may reach up to $\sim 500\ \mathrm{cm}^{-1}$ that are not negligible compared to the magnitude of the total Stokes shift, i.e., $\sim 3500\ \mathrm{cm}^{-1}$. (iv) In HOCs and RHOCs, the time scales describing the latter slow dynamical modes are all well beyond the nanosecond time domain whereas in HICs, as a consequence of the somewhat weaker wall-probe coupling, they may drop down to the subnanosecond temporal regime.

The general picture that emerges from the previous considerations would confirm that the overall solvation response in confined environments would not only reflect modifications of the spatial and orientational arrangement of the solvent that follow a sudden change in the electronic distribution of the probe but would be also modulated by modifications in the spatial and orientational degrees of freedom of the probe itself.[21] In principle, the dynamics of the latter fluctuations would be independent of the vertical excitation process and would involve time scales that are, at least, between 1 and 2 orders of magnitude larger than those characterizing the dynamical modes of most of solvent molecules. As such, and for all practical purposes, the decay of $S(t)$ shown in Figure 8 would provide information mostly about solvent dynamical modes. Should this line of reasoning be correct, the previous argument could be invoked to explain why the solvent response in RHOCs is somewhat faster: note that the embedding of the probe within a wall domain surrounded by TMS groups, would render the solvent response localized mostly at more central regions of pore, i.e., in the vicinity of the C11−O19, carbonyl group, where retardation effects are milder (see plots of $\rho^{\alpha}(r)$ for coumarin sites in Figure 6c). By contrast, the closest solvation shells of the coumarin in HOCs and HICs would mostly include molecules lying in more external, and consequently slower, solvent layers, bringing moderate increments in τ_{slv}.

IV. CONCLUDING REMARKS

In this paper, we have examined microscopic characteristics pertaining to the solvation of a fluorescent probe in MeOH, within three different silica pores with diameters close to ∼3 nm. To asses the effects derived from the functionalization at the pore walls, we have analyzed three environments with different degrees of hydrophobicity and wall-roughness. Given the inherent spatial inhomogeneities of the solvation environment, special care was taken to incorporate full atomistic detail in our model Hamiltonian. In doing so, we tried to capture the different effects in the solvation originated in the diversity of relevant length scales of the problem under investigation.

Concerning the spatial localization of the probe within the hydrophobic pores, our simulation results reveal the prevalence of wall-solvation states, characterized by a parallel alignment of the molecular plane of the probe in close contact with the solid interface. Under such circumstances, the only relevant dynamical modes observed were in-the-wall rotations, interrupted by much more rare episodes corresponding to out-of-the-wall flips. Note that this segregation toward the interface is akin to similar processes observed in sparingly soluble species at water−air interfaces[43] and is benefited not only from energetic but also from entropic considerations. Upon partial hydroxylation of the pore wall, the solvation of coumarin becomes bistable, with

alternations between wall-like and bulk-like solvation states. Compared to what we observed in hydrophobic pores, wall states are characterized by a partial detachment of the probe from pore-wall which, in turn, remains preferentially coated by a tightly bound layer of solvent molecules. Moreover, the weakening of the wall-probe coupling also allows for full detachment episodes, followed by the partial stabilization of the probe at central regions of the pore. Finally, the partial restoration of the original hydrophobicity, along with a sensible increment in the wall-roughness leads to a completely different scenario, in which the probe remains adsorbed to a wall domain surrounded by TMS groups. This "anchoring" leads to the suppression of diffusive motions in the time scale of several tens of nanoseconds and also to severe restrictions in the overall rotational dynamics, which can be described in terms of restrained angular motions with amplitudes that do not surpass ∼20°.

We have also recorded the initial stages of relaxation of the solvent energy gap upon a vertical excitation of the probe for about ∼30 ps. In pore environments, the characteristic time scales were intermediate between 2 and 4.5 times longer than the one describing similar relaxations in the bulk, with the following fast-to-slow trend: RHOC→HOC→HIC. The geometrical characteristics of the prevailing solvation states in each pore provide a simple interpretation of this tendency: In RHOCs, a sizable fraction of the probe "surface" remains in contact with TMS groups, whereas the solvent response comes mostly from a first solvation shell localized in more central—and consequently, faster—pore domains. By contrast, in HIC and HOC, the vast majority of the MeOH molecules comprising the first solvation shell is located in outer—and consequently, more sluggish—pore regions, a fact that would bring the overall response somewhat slower. Of course, beyond this first initial temporal regime, the relaxation of $\Delta E(t)$ should also be modulated by dynamical modes associated to modifications in the spatial and orientational characteristics of the solvation state. Yet, such contributions are described by time scales that are exceedingly long to be properly captured by our nonequilibrium simulation experiments.

In the introductory section, we made reference to time-resolved fluorescence experiments for the solvation of confined ethanol in sol−gel glasses[12] and silica pores.[13] Despite the obvious differences in the solvent considered, the comparison between the direct experimental information and the present results is not straightforward for several reasons. First, the time scales and the Stokes shifts reported from the two set of experiments differ in a sensible fashion. Moreover, the lack of agreement not only involves results for confined probes, but they also persist in the bulk case and could be ascribed to time resolution limitations of the experimental setups.[13] Leaving aside for a moment these discrepancies, the retardations in the rotational motions of the confined probes reported here—a factor of 10−30 in τ_{rot}—are exceedingly large compared to those reported by Baumann: $\tau_{rot} \approx 75 \pm 4$ ps in pores vs $\tau_{rot} \approx 67 \pm 1$ ps in the bulk. Concerning τ_{slv}, the differences between bulk and confined results compare much better with our predictions since the solvation characteristic times for pores are twice as long as those in the bulk. Additional simulations, stretching the temporal time domain investigated is surely called for to reconcile our predictions with direct experimental information.

Nevertheless, we are confident that the arguments presented in the previous paragraphs provide new evidence supporting the hypothesis that suggests that signals from time-resolved Stokes shifts measurements in these inhomogeneous systems not only provide information about modifications operated in the dynamical modes of solvent upon confinement but also reveal modifications in the prevailing solvation structures which, in principle, may not be directly connected with the electronic excitation of the probe.

AUTHOR INFORMATION

Corresponding Author
*E-mail: DoloresElola@gmail.com.

ACKNOWLEDGMENT

This work was partially funded by ANPCyT (Grants PICT2007-00300 and PICT2007-00334). Financial support from BID-PAE No 22711 is gratefully acknowledged. M.D.E., J.R., and D.L. are staff members of CONICET (Argentina).

REFERENCES

(1) Jinesh, K. B.; Frenken, J. W. M. *Phys. Rev. Lett.* **2008**, *101*, 036101.
(2) Angell, C. A. *Science* **2008**, *319*, 582.
(3) Rasaiah, J. C.; Garde, S.; Hummer, G. *Annu. Rev. Phys. Chem.* **2008**, *59*, 713.
(4) Jarzeba, W.; Walker, G. C.; Johnson, A. E.; Barbara, P. F. *Chem. Phys.* **1991**, *152*, 57.
(5) Horng, M. L.; Gardecki, J. A.; Papazyan, A.; Maroncelli, M. *J. Phys. Chem.* **1995**, *99*, 17311.
(6) Horng, M. L.; Gardecki, J. A.; Maroncelli, M. *J. Phys. Chem. A* **1997**, *101*, 1030.
(7) Chakrabarty, D.; Chakraborty, A.; Seth, D.; Hazra, P.; Sarkar, N. *Chem. Phys. Lett.* **2005**, *412*, 255.
(8) Kometani, N.; Hoshihara, Y.; Yonezawa, Y.; Kajimoto, O.; Hara, K.; Ito, N. *J. Phys. Chem. A* **2004**, *108*, 9479.
(9) Chakrabarty, D.; Chakraborty, A.; Seth, D.; Hazra, P.; Sarkar, N. *Chem. Phys. Lett.* **2004**, *397*, 469.
(10) Jin, H.; Baker, G. A.; Arzhantsev, S.; Dong, J.; Maroncelli, M. *J. Phys. Chem. B* **2007**, *111*, 7291.
(11) Hazra, P.; Chakrabarty, D.; Chakraborty, A.; Sarkar, N. *Biochem. Biophys. Res. Commun.* **2004**, *314*, 543.
(12) Baumann, R.; Ferrante, C.; Kneuper, E.; Deeg, F.-W.; Bräuchle, C. *J. Phys. Chem. A* **2003**, *107*, 2422.
(13) Kamijo, T.; Yamaguchi, A.; Suzuki, S.; Teramae, N.; Itoh, T.; Ikeda, T. *J. Phys. Chem. A* **2008**, *112*, 11535.
(14) Elola, M. D.; Rodriguez, J.; Laria, D. *J. Chem. Phys.* **2010**, *133*, 154707.
(15) Maroncelli, M. *J. Mol. Liq.* **1993**, *57*, 1.
(16) Rosenthal, S. J.; Jimenez, R.; Fleming, G. R.; Kumar, P. V.; Maroncelli, M. *J. Mol. Liq.* **1994**, *60*, 25.
(17) Kumar, P. V.; Maroncelli, M. *J. Chem. Phys.* **1995**, *103*, 3038.
(18) Bagchi, B. *Annu. Rev. Phys. Chem.* **1989**, *40*, 115.
(19) Hynes, J. T. *Ultrafast Dynamics of Chemical Systems*; Simon, J. D., Ed.; Kluwer: Dordrecht, Netherlands, 1994.
(20) Thompson, W. H. *J. Chem. Phys.* **2002**, *117*, 6618.
(21) Thompson, W. H. *J. Chem. Phys.* **2004**, *120*, 8125.
(22) Feng, X.; Thompson, W. H. *J. Phys. Chem. C* **2007**, *111*, 18060.
(23) Morales, C. M.; Thompson, W. H. *J. Phys. Chem. A* **2009**, *113*, 1922.
(24) Feng, X.; Thompson, W. H. *J. Phys. Chem. C* **2010**, *114*, 4279.
(25) Faeder, J.; Ladanyi, B. M. *J. Phys. Chem. B* **2001**, *105*, 11148.
(26) Rodriguez, J.; Mart, J.; Guàrdia, E.; Laria, D. *J. Phys. Chem. B* **2008**, *112*, 8990.
(27) Gulmen, T. S.; Thompson, W. H. *Dynamics in small confining systems VIII*; Fourkas, J. T., Levitz, P., Overney, R., Urbakh, M., Eds.; Materials Research Society Symposium Proceedings: Warrendale, PA, 2006; Vol. 899E.

(28) Rodriguez, J.; Elola, M. D.; Laria, D. *J. Phys. Chem. B* **2010**, *114*, 7900.
(29) MacKerell, J. A. D.; Banavali, N.; Foloppe, N. *Biopolymers* **2001**, *56*, 257.
(30) Martins, L. R.; Skaf, M. S. *Chem. Phys. Lett.* **2003**, *370*, 683.
(31) Moylan, C. R. *J. Phys. Chem.* **1994**, *98*, 13513.
(32) Baumann, W.; Nagy, Z. *Pure Appl. Chem.* **1993**, *65*, 1729.
(33) Phillips, J. C.; Braun, R.; Wang, W.; Gumbart, J.; Tajkhorshid, E.; Villa, E.; Chipot, C.; Skeel, R. D.; Kale, L.; Schulten, K. *J. Comput. Chem.* **2005**, *26*, 1781.
(34) The results displayed in Figure 7 correspond to orientational fluctuations measured with respect to the dipole moment in the S_0 state. This description should be equivalent to the one provided by the transition dipole moment.
(35) Barbara, P. F.; Jarzeba, W. *Adv. Photochem.* **1990**, *15*, 1.
(36) Castner, E. W., Jr.; Maroncelli, M. *J. Mol. Liq.* **1998**, *77*, 1.
(37) Maroncelli, M. *J. Chem. Phys.* **1991**, *94*, 2084.
(38) Maroncelli, M.; Fleming, G. R. *J. Chem. Phys.* **1988**, *89*, 5044.
(39) Carter, E. A.; Hynes, J. T. *J. Chem. Phys.* **1991**, *94*, 5961.
(40) Fonseca, T.; Ladanyi, B. M. *J. Mol. Liq.* **1994**, *60*, 1.
(41) Furse, K. E.; Corcelli, S. A. *J. Am. Chem. Soc.* **2008**, *130*, 13103.
(42) Baumann, R; Ferrante, C.; Deeg, F. W.; Bräuchle, C. *J. Chem. Phys.* **2001**, *114*, 5781.
(43) Pantano, D.; Laria, D. *J. Phys. Chem. B* **2003**, *107*, 2971.